JOURNAL OF GEOPHYSICAL RESEARCH, VOL. 112, A09304, doi:10.1029/2006JA011794, 2007

Click Here for Full Article

Ground and satellite observations of the evolution of growth phase auroral arcs

M. R. Lessard,[1] W. Lotko,[2] J. LaBelle,[3] W. Peria,[4] C. W. Carlson,[5] F. Creutzberg,[6] and D. D. Wallis[7]

Received 18 April 2006; revised 28 March 2007; accepted 26 April 2007; published 8 September 2007.

[1] Auroral substorms are the result of a complex process involving coupling between the solar wind, magnetosphere and ionosphere. In this study, the objective is to understand the processes that precede what is perhaps the most fundamental aspect, the brightening of a preexisting arc at onset. The notion that this brightening provides an indicator of substorm onset remains one of the few aspects of substorms that is not disputed. In order to understand the processes that lead up to onset, auroral arcs that form during substorm growth phases are examined using ground-based (CANOPUS) data with in situ measurements acquired by the FAST satellite. Four cases have been studied and are discussed in detail here. Consistent with other reports, the data show that the growth phase arcs persist for 30 min or more. During this time, the arcs often show little or no fluctuations, although a gradual intensification is clear in the ground-based optical measurements. Two important results emerge from this study. First, FAST observations show that growth phase arcs develop within the region of proton precipitation but generally poleward of most intense precipitation, a topic that has been addressed (and disputed) using ground-based observations of luminosity, a secondary effect. Second, we show that FAST observations before the growth phase arc is established show scattered plasma sheet electrons with no significant structure. However, once the growth phase is well developed, FAST confirms that the arcs are excited via inverted V precipitation, implying that an inverted V potential drop gradually develops in conjunction with the evolution of the growth phase.

Citation: Lessard, M. R., W. Lotko, J. LaBelle, W. Peria, C. W. Carlson, F. Creutzberg, and D. D. Wallis (2007), Ground and satellite observations of the evolution of growth phase auroral arcs, *J. Geophys. Res.*, *112*, A09304, doi:10.1029/2006JA011794.

1. Introduction

[2] *Akasofu* [1964] proposed that substorms occur according to a certain sequence, beginning with the brightening of a preexisting auroral arc and ending with a recovery phase. *McPherron* [1970] and *Pudovkin et al.* [1970] extended this work to include the notion of a growth phase, where energy is stored in the magnetotail before being released at substorm onset. During a substorm growth phase, auroral arcs observed on the ground are known to migrate equatorward. This motion is thought to be associated with a stretching of the nightside magnetotail as a result of an enhanced transfer of solar wind energy to the magnetosphere [*McPherron*, 1970]. Following slow growth, substorm onset is then observed as a brightening of the preexisting arc as described by *Akasofu* [1964, 1968]. Accordingly, the nature of this arc likely determines to what extent certain physical processes can occur at onset and thus should place constraints on the initial conditions for substorm models (see discussions by *Kamide* [2001] and *Lui and Murphree* [1998]). Of course, other arcs are often present before onset that likewise provide some degree of coupling. The relative significance of these arcs is likely related to the fact that the equatorward arc is tied to the inner edge of the plasma sheet, where the significant gradients may provide a pathway for energy transfer. In fact, recent work using IMAGE and FAST data (S. Mende, personal communication, 2006) show observations of Alfvenic aurora at onset (in the region of the preexisting arc), suggesting that compressional wave power travels from deeper in the tail to provide this energy.

[3] Of course, substorms have onset signatures besides the brightening of a preexisting arc. These signatures include dipolarization at geosynchronous orbit, a decrease in the northward component of the magnetic field observed

[1]Space Science Center, University of New Hampshire, Durham, New Hampshire, USA.
[2]Thayer School of Engineering, Dartmouth College, Hanover, New Hampshire, USA.
[3]Department of Physics, Dartmouth College, Hanover, New Hampshire, USA.
[4]Department of Earth and Space Sciences, University of Washington, Seattle, Washington, USA.
[5]Space Sciences Laboratory, University of California, Berkeley, California, USA.
[6]Keometrics, Ottawa, Ontario, Canada.
[7]Magnametrics, Ottawa, Ontario, Canada.

Copyright 2007 by the American Geophysical Union.
0148-0227/07/2006JA011794$09.00

on the ground (a negative bay), Pi2 and Pi1B pulsations and energetic particle injections at geosynchronous orbit. However, the brightening of a preexisting arc is the only onset signature that can also provide information before substorm onset as well. In particular, the preexisting arc indicates the existence of a specific region of magnetosphere-ionosphere coupling before onset, since the arc itself is essentially the manifestation of an acceleration region at higher altitudes with a particle source region that maps to the plasma sheet. At onset, the initial release of energy from the magnetosphere to the ionosphere is invariably directed along these flux tubes.

[4] Visually, auroral emissions at high latitudes in the dusk sector (before the start of a substorm growth phase) consist of 5577 Å emissions, which are generally thought to be evidence of scattered plasma sheet electrons impacting the upper atmosphere. However, scanning photometer data also show the presence of 4861 Å emissions that map to the same latitude, which are generally attributed to proton precipitation. *Fukunishi* [1975] showed that, in the case of diffuse aurora during quiet times, a significant fraction of 5577 Å emissions can result from energetic proton precipitation. Specifically, they showed that the ratio of I(5577 Å)/$I(\mathrm{H}\beta)$ during such periods is typically 10, in agreement with theoretical predictions by *Eather* [1967]. *Fukunishi* [1975] goes on to conclude that the precipitating particles in this region are primarily protons.

[5] The arc that brightens at onset, however, is generally thought to be a narrower, well-defined structure as opposed to diffuse 5577 Å emissions. *Fukunishi* [1975] studied scanning photometer data to compare proton and electron emissions during various local times. They conclude that, while these emissions are separated in the evening to midnight regions, they overlap after midnight. *Vallance Jones et al.* [1985], also using a chain of scanning photometers, conclude that the peak in proton emissions is equatorward of the electron emissions before onset. However, in each of the examples they show (which are from the premidnight sector), the electron and proton emissions clearly do overlap in latitude. The strongest statement that electron aurora is coincident with proton aurora during a growth phase is presented by *Samson et al.* [1992], who conclude that the arc that brightens at substorm onset is an electron arc embedded in the same region as the diffuse proton aurora. In this study, we show that, while the electron precipitation does tend to be poleward of the proton precipitation during a growth phase, high-resolution ground-based scanning photometer data, confirmed with data from the FAST satellite, show that these precipitation regions do overlap significantly. This scenario suggests that the well-defined arc that eventually brightens at onset develops gradually within some region of the diffuse aurora.

[6] Recently, *Lyons et al.* [2002] emphasized that, at least for the cases they considered, an additional "breakup arc" forms just a few minutes (~4) before onset just equatorward of the existing arc and that this is the arc that subsequently brightens at onset. Similar sequences of arc formation had also been mentioned by *Akasofu* [1968], *Erickson et al.* [2000], and *Maynard et al.* [1996]. However, a recent study of 33 substorms by *Deehr and Lummerzheim* [2001] did not find this to be the case and, in fact, found that the arc that brightened typically was poleward of the arc at the plasma sheet trapping boundary, a conclusion that would apparently contradict that of *Lyons et al.* [2002]. *Bristow et al.* [2003] examined an isolated growth phase and, although no newly formed breakup arc was observed in their study, the presence of enhanced plasma flows ~5 min before the arc brightening were noted by the authors. Finally, fading of growth phase arcs before onset has been discussed by several authors [see *Kauristie et al.*, 1997; *Safargaleev et al.*, 1997, and references therein].

[7] Clearly, a variety of phenomena can occur during the minutes just before onset, and, while these changes may be important, this work concentrates on the slower development of growth phase arcs and, specifically, examines the evolution from the observed diffuse aurora to a growth phase arc using a combination of CANOPUS and FAST data.

[8] In this paper, the two most significant results have to do with (1) the location of the growth phase arc relative to proton precipitation and (2) the nature of the evolution of growth phase arcs, and in particular, the fact that inverted V arcs during the growth phase develop gradually from scattered plasma sheet electron precipitation.

2. Data and Analysis

[9] The objective of this study is to quantify properties of auroral arcs during substorm growth phases, focusing specifically on the arc that brightens at substorm onset. These arcs are, without exception, quiet arcs in the sense that changes occur slowly (over the course of tens of minutes). A number of studies of quiet arcs have been carried out, and most of these studies likely occurred during a substorm growth phase, but in this case, the context of a substorm growth phase is an important criteria in the event selection.

[10] A substorm growth phase is a phenomena that lacks a widely accepted, detailed definition. Most observers would agree that a "canonical" scenario includes the equatorward drift of a quiet arc over perhaps 30–60 min, to be followed (at onset) by the brightening of that arc, a description that is consistent with the original definition presented by *McPherron* [1970]. Since the objective of this study has been to quantify parameters of these arcs, event selection began with this basic definition, although further constraints (described below) were imposed in order to study "clean" events, i.e., those that were well-isolated and that have good data.

[11] The primary ground station in this study is the CANOPUS site in Gillam, Manitoba, located at a geographic latitude of 56.2°N, a longitude of 94.4°W and a magnetic latitude of 67.1° (see Figure 1). As much as possible, events were selected that also had FAST overflights in order to compare the ground-based measurements with in situ data. However, the task of finding FAST flights over Gillam when a well-defined growth phase arc is present (without clouds, etc.) has proven to be quite difficult and the events considered in this study represent the best available events from four seasons (i.e., four winters) of data.

[12] The scanning photometer data used in this study were acquired using with a high-resolution mode of the instrument, where data were acquired in 80 bins (instead of the usual 17 bins) as the field of view was swept overhead, nominally from horizon to horizon. The result is that the

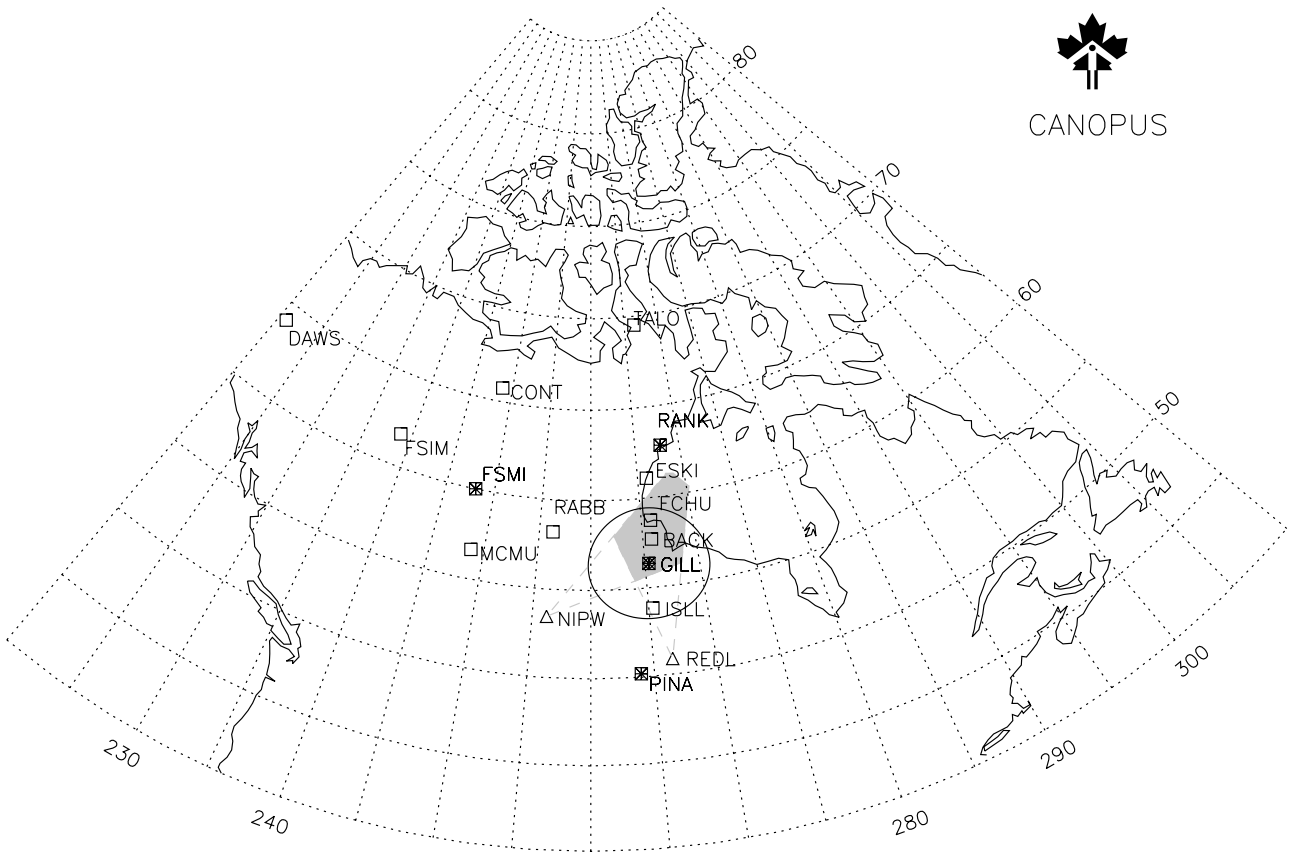

Figure 1. The CANOPUS array of ground stations. The data used in this study were obtained at stations along the Churchill-Gillam meridian. The circle in the center of the map shows the field of view of the Gillam all-sky camera. The magnetic latitude at Gillam is 67.1°.

spatial resolution of the instrument is limited by its field of view, which is 4°, providing a spatial resolution better than 10 km near zenith (as opposed to the usual 50 km resolution used in past studies that used CANOPUS scanning photometer data). In calculating the magnetic latitudes of the emissions, an AACGM model was used with assumed altitudes of 230 km for 6300 Å emissions and 110 km for all others.

[13] Specific event selection criteria is as follows. Growth phase arcs were nominally identified using scanning photometer data. The particular signature that was sought was that of an isolated arc with a gradual equatorward drift, followed by an abrupt poleward motion. In all cases, the interpretation of this sequence as a substorm growth phase was reinforced by the subsequent occurrence of a negative bay in the north–south component of the magnetic field, the signature of an east–west electrojet overhead. In addition to this basic selection criteria, further constraints on event selection were imposed in order to insure that the events were well isolated, with the intent that other (unrelated) geophysical phenomena did not "contaminate" this study. To summarize:

[14] 1. Each event shows a distinct equatorward motion of an arc in scanning photometer data. Note, in particular, that the equatorward drift of the 4861 Å emissions southward boundary can be directly associated with magnetotail stretching [*Donovan et al.*, 2003], as typically occurs during a growth phase.

[15] 2. Each event shows onset occurring within 2° of local zenith. This condition was imposed so that fluctuations in luminosity would not be obscured by viewing a structure that was too low on the horizon.

[16] 3. Each event was preceded by at least three hours of minimal magnetic activity, defined as fluctuations with amplitudes of $\leq$40 nT in the X-component at Gillam.

[17] 4. Finally, each growth phase was followed by a distinct substorm onset as indicated by the presence of a negative bay in a fluxgate magnetometer. Since a negative bay is the signature of an electrojet and is not necessarily colocated with the growth phase arc, the requirement was only that it formed along the Churchill-Gillam meridian. Because isolated growth phases and onsets were preferred, a few of the events that were considered showed a relatively weak electrojet signature, as low as 80 nT.

[18] On the basis of the above criteria, four events were selected for inclusion in the study, three of which have FAST data that correspond to the ground-based observations. Intervals of diffuse aurora that typically occur before (in MLT as well as UT) the beginning of a growth phase were specifically excluded. Diffuse aurora, observed in conjunction with scattered plasma sheet electrons, is a well-known phenomenon and is to be distinguished from growth phase arcs, which we conclude evolve gradually

Table 1. Events Used for This Study[a]

Date, yymmdd	FAST	Onset, UT	Int, nT	Fluctuations, mHz
990119	N/A	0530	260	-
970109	1523	0718/0750	460	0.002
990206	9733	0528	280	-
970926	4335	0643	80	-

[a]The second column lists the FAST orbits relevant for each event; the third column lists the onset time determined by a sharp drop in the X (north-south) component of the magnetometers along the meridian; the fourth column shows the strength of the perturbation (i.e., the strength of the westward electrojet). Note, however, that the actual onset time for the first event (990119), as determined using Polar UVI data, is closer to 0520 UT.

from the diffuse aurora. Information regarding the specific events is listed in Table 1. Four of the events are discussed in detail in this paper in order to illustrate the following points:

2.1. Event 1: 19 January 1999

[19] Figure 2 shows scanning photometer data from the CANOPUS site in Gillam, Manitoba. Emissions at 4861 Å 5577 Å and 6300 Å are plotted with AACGM latitude [*Baker and Wing*, 1989] along the vertical axis, time along the horizontal axis and intensity represented by the color scale. In the 5577 Å and 6300 Å panels, the black lines track the brightest pixels during the growth phase. The lower black line in the 4861 Å panel tracks the brightest pixels at 4861 Å but the upper trace is simply copied from the 5577 Å channel. In other words, the data show that 5577 Å emissions are approximately 1° poleward of the 4861 Å for this event (this is discussed in more detail below). No all-sky data were available for this event, although Polar UVI data show that onset occurred approximately 1 hour east of Gillam, at approximately the same latitude, but near 0520 UT. An important point, demonstrated below, is that the arc (in this example, as well as each of the others) gradually intensified, implying that M-I coupling was enhanced during the growth phase in that region. On the other hand, the actual onset occurred somewhat to the east, where nothing is known about the evolution of arc. Thus it may be case that there is no significant difference between an arc that resides somewhat outside the actual onset region and the arc that actually precedes the global onset appearing in the same MLT sector.

[20] For each wavelength, the data along the black line (the brightest pixels) are extracted and plotted versus time in the smaller panel beneath the colored panel. The small panel to the right is the Fourier transform of the extracted data, presented to show the frequencies of any fluctuations that may be present.

[21] This first event is presented as a "clean" example of a growth phase arc, in the sense that it provides as simple an example of a growth phase as can be expected. The specific start time of the growth phase is difficult to identify, as it is with most of the events we considered. However, equatorward motion can be seen to begin gradually near 0400 UT, followed by onset at ~0520 UT, yielding a growth phase of 80 min, which is typical of the events considered in this study. Note, also, the fading before onset that occurs near 0455–0505 UT. From these data alone, two important points can be made. First, the line plots of extracted data show that the arc is void of periodic fluctuations (that might be present if the arc was energized or modulated by an Alfvén wave). Second, the persistence of the arc throughout the growth phase is clear, showing long-lived stationarity of the emissions.

[22] Figure 3 shows the ratio of 5577 Å to 6300 Å emissions (using data extracted along the black lines). This ratio can be used as a proxy for the incident electron energy as described by *Steele and McEwen* [1990]. Basically, the 5577 Å emissions are excited by higher energy (~1 keV or greater) electrons, while the 6300 Å are excited by those with a few hundred eV. In this study, only the relative intensities of the emissions are considered. For example, if the ratio of the emissions is seen to increase, then the

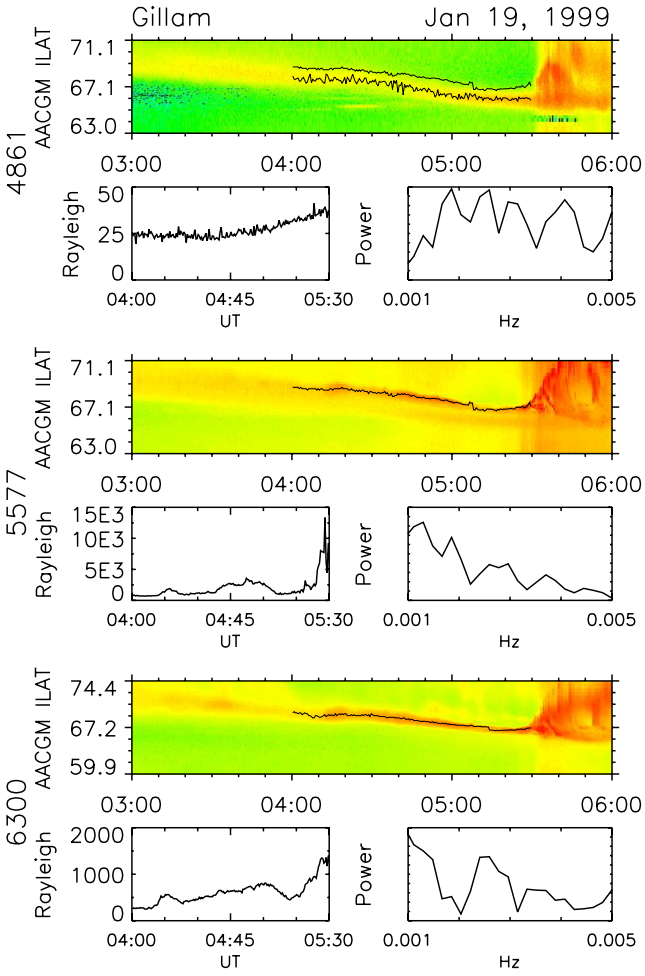

Figure 2. Scanning photometer data acquired at Gillam, Manitoba. Data at three wavelengths are shown: 4861, 5577, and 6300 Å. For each wavelength, the upper panel shows emission intensities with magnetic latitude plotted along the vertical axis and time along the horizontal axis. The black trace in the 5577 and 6300 channels track the brightest pixel as a function of time. Two traces are shown in the 4861 channel. One (the equatorward one) tracks the brightest pixels in that channel; the other trace is simply copied from the 5577 channel to highlight any separation in latitude that might be present. Below each colored panel, data extracted along the trace are plotted versus time with the Fourier spectrum of that data plotted to the right.

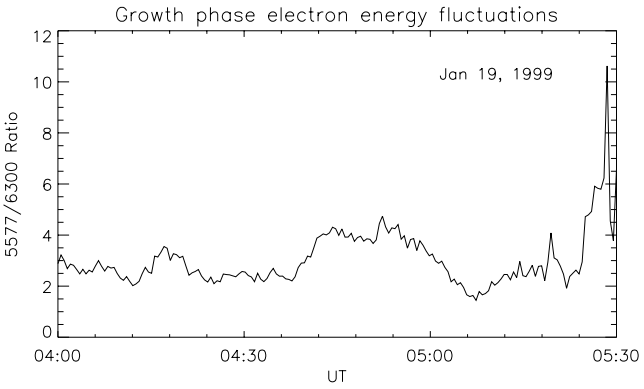

Figure 3. The ratio of 5577 to 6300 Å emissions during the time highlighted as shown in Figure 2. This ratio serves as a proxy to show relative changes in the energy of the precipitating electrons.

interpretation is that a change has occurred that has resulted in the precipitation of more energetic electrons. In Figure 3, there is no significant change (until 0520 UT at substorm onset), and the incident electron energy is taken to be relatively constant. At the same time, however, a distinct increase in 5577 Å and 6300 Å emissions can be seen in the middle and bottom panels in Figure 2, beginning near 0415 UT and continuing until just after 0500 UT. This increase in the luminosity of these emissions indicates an increase in the incident particle flux, indicative of a gradual intensification of the arc.

[23] Returning to the top panel in Figure 2, note that a clear latitudinal separation between the 4861 Å and the 5577 Å emissions is apparent. While this result is consistent with that of *Fukunishi* [1975], *Vallance Jones et al.* [1985], and *Deehr and Lummerzheim* [2001] in that it shows a separation between the regions of electron and proton precipitation, it contrasts with that of *Samson et al.* [1992], who conclude that substorm intensification begins as the brightening of an electron arc that is embedded in a region of energetic proton precipitation. In any case, FAST data for some of the events considered in this study (below) show that the electron precipitation often does overlap the proton precipitation (in latitude), but has a centroid that is typically poleward of the protons, at least for the events considered here. This last point is important because FAST measures the actual particle precipitation directly, as opposed to the luminosity that results from this precipitation. We note that recent work by *Yago et al.* [2005] uses DMSP data to also show that the regions of electron and precipitation overlap.

[24] Finally, note that in the center (5577 Å) panels of Figure 2, an additional arc appears to form 1° equatorward of the black line that traces the brightest emissions. This, in fact, is not an actually an arc that can be attributed directly to energetic electrons, but luminosity that results in conjunction with the proton precipitation as shown in the 4861 Å channel, as described by *Fukunishi* [1975] and discussed above. In Figure 2, this idea is also supported by noting that the intensification of what appears to be an equatorward arc (5577 Å emissions) at ~0445 UT coincides precisely with the intensification in the 4861 Å channel, seen most clearly in the extracted data. Intensification of 4861 Å emissions during substorm growth has also been noted by *Deehr and Lummerzheim* [2001] and *Voronkov et al.* [1999] and is generally attributed to increased thinning of the plasma sheet and an associated increase in the number of scattered protons.

2.2. Event 2: 9 January 1997

[25] Figure 4 shows data from 9 January 1997, plotted in the same format as the first event. As in the first event, the data in the 5577 Å channel that were extracted along the most luminous pixels show no periodic fluctuations during the growth phase. In the 6300 Å channel, however, very faint fluctuations with a frequency of 0.002 Hz are barely detectable, although the technique of tracking the brightest pixels in this case results in selecting pixels that are clearly outside the growth phase arc. As in the previous example, we conclude that the growth phase arc is essentially stationary (except perhaps for a slow drift), i.e., that it has no significant fluctuations in luminosity. In contrast with the previous example, emissions in the 5577 Å channel increase fairly abruptly near 0625 UT. All-sky camera data (not shown) indicate that the initial brightening (near 0718 UT) occurred just to the west of the station, although the full onset (at 0744 UT) occurred directly overhead. This is

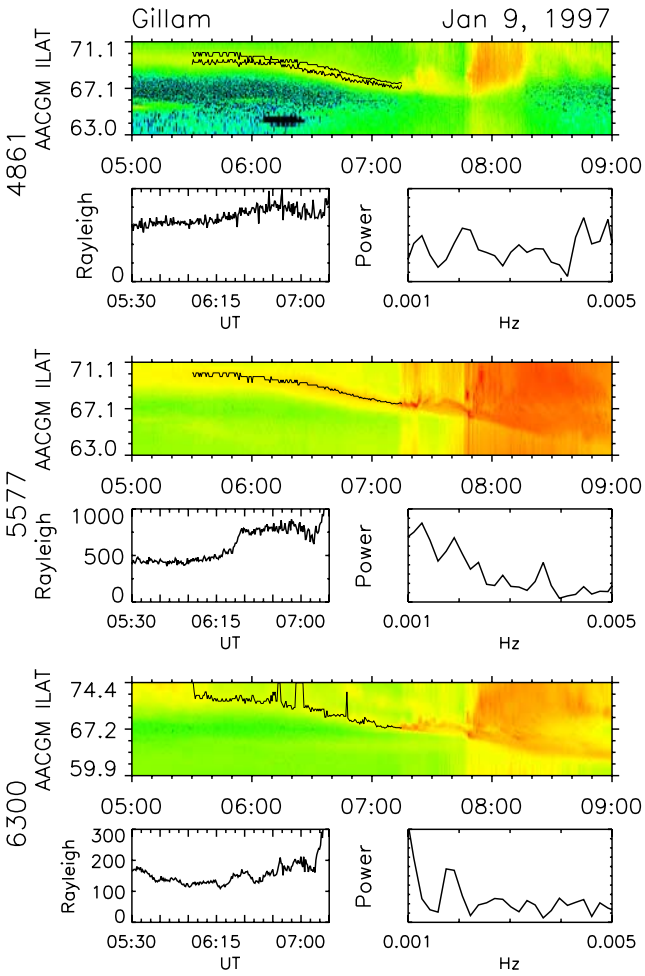

Figure 4. Scanning photometer data for the event on 9 January 1997, plotted in the same format as in Figure 2.

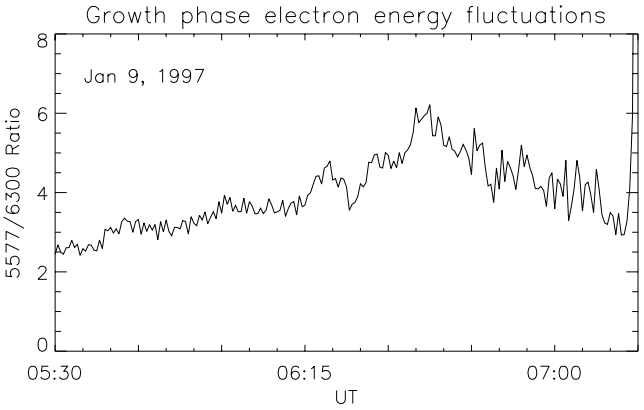

Figure 5. The ratio of I(5577 Å)/I(6300 Å) emissions for 9 January 1997.

confirmed with Polar UVI images, as well as with electrojet signatures in CANOPUS magnetometers.

[26] The I(5577 Å)/I(6300 Å) ratio was calculated and is plotted in Figure 5. In spite of the abrupt nature of the increase in 5577 Å emissions, the ratio increases gradually until 0640 UT, when it decreases, apparently due to an increase in 6300 Å luminosity. The increase in luminosity (in both channels, although at separate times) with an increase in the I(5577 Å)/I(6300 Å) ratio implies an increase in incident electron energy flux and and accompanying increase in electron energy, an indication of a gradual increase in the total incident particle energy flux. Also, note that as in the first example, the intensity of 4861Å emissions also increases gradually.

[27] Finally, we again copy the black trace from the extracted 5577 Å emissions onto the 4861 Å emissions in order to compare the invariant latitude of these signatures. Although the traces appear to almost overlap, the latitudinal separation between the peaks in the emissions is almost 1° and is verified by FAST observations (although the proton and electron precipitating regions do overlap in latitude).

[28] Figure 6 shows electron and ion data from the FAST satellite as it traversed nominally poleward, along a meridian approximately 1 hour to the east of Gillam. The arrow in Figure 4 shows when this occurred. On the basis of the apparent stability of the aurora, however, a reasonable assumption is that the FAST observations coincide with the Gillam photometer data. The top panel shows electron energy fluxes; the second panel shows pitch angles of electrons with energies above 100 eV; the third panel shows ion energy fluxes; and the bottom panel shows pitch angles of ions with energies above 10 eV. The burst-like artifacts seen in the data presented here and in other FAST plots result from mode changes of the instruments and should be ignored.

[29] In Figure 6, plasma sheet ions ($\sim 10^4$ eV, observed from 0618:00 to 0618:30 UT) are visible as FAST passes through 69° invariant latitude, which maps well to the 4861 Å emissions shown in Figure 4. Note that the luminosity at 4861 Å spans approximately 1° in latitude as observed from the ground, while the in situ measurements of FAST show that the proton precipitation region actually spans ~1.6°. Electrons with energies just above 1 keV are collocated with these ions or perhaps slightly poleward. Then, near the poleward boundary of the scattered electrons (at ~0618:50), a weak inverted V signature is present, marked with an arrow in the figure, which maps precisely to the growth phase arc seen in the scanning photometer data. This arc has a latitudinal width of ~1° as observed both on the ground and by FAST. The relative location of the plasma sheet ions and the weak inverted V coincide well with the two black traces in the upper panel of Figure 4, showing that the growth phase arc is developing just slightly poleward of the peak in plasma sheet ion precipitation. Note, also, that the weak inverted V at ~0620:10 is well poleward of Gillam and is not the arc that brightened at onset.

[30] Two related points should be mentioned here. The first is that in cases where Gillam passed through the local midnight sector without the occurrence of a substorm, FAST observations did not show inverted V precipitation (see the example on 26 September 1997 below). In cases where FAST traversed over the arc later in the growth phase, a more distinct inverted V was present (examples are shown below). On the basis of data from this event and the others included in the study, a conclusion to be drawn is that before a growth phase begins, the aurora in the vicinity of the growth phase "arc" is excited simply by scattered plasma sheet electrons. Then, as the growth phase develops, an inverted V signature gradually forms, coincident with the intensification of the arc.

2.3. Event 3: 6 February 1999

[31] Figure 7 shows scanning photometer data plotted in the same format as in the first two events. As in the previous events, the arcs as seen in the 5577 Å and 6300 Å data appear to be relatively stationary and persistent, although perhaps with some quasi-periodic fluctuations in the 5577 Å channel. The associated all-sky camera data show this arc to be the one that eventually brightened at onset. We emphasize that the magnetometer data show the strongest electrojet signatures along the Churchill line, although it is not possible to definitively determine the precise location of onset, either from the all-sky camera data or otherwise. It may the case that onset occurred some distance away, as is the case in the first event.

[32] Also, the gradual brightening in all three channels supports the notion that the arc is intensifying throughout the growth phase. Figure 8 shows the I(5577 Å)/I(6300 Å) ratio, which indicates an increase in the precipitation energy. As in the second event, the data show both an increase in luminosity as well as an increase in the incident electron energy, indicating a gradual increase in the total incident particle energy flux.

[33] Next, data derived from the Gillam all-sky camera data are presented in Figure 9. The traces in the figure were extracted from individual frames of all-sky data by selecting the brightest pixel along the north-south direction. Essentially, then, the traces represent the brightness of the arc from east to west. This process was carried out for two different times, chosen to represent the arc in the early (black trace, 0400 UT) and later (red trace, 0459 UT) stages of the growth phase. The top panel in the figure shows data from the 5577Å image; the second panel shows data from the 6300Å image. The third panel shows the sum of these emissions, used to represent the relative total precipitation

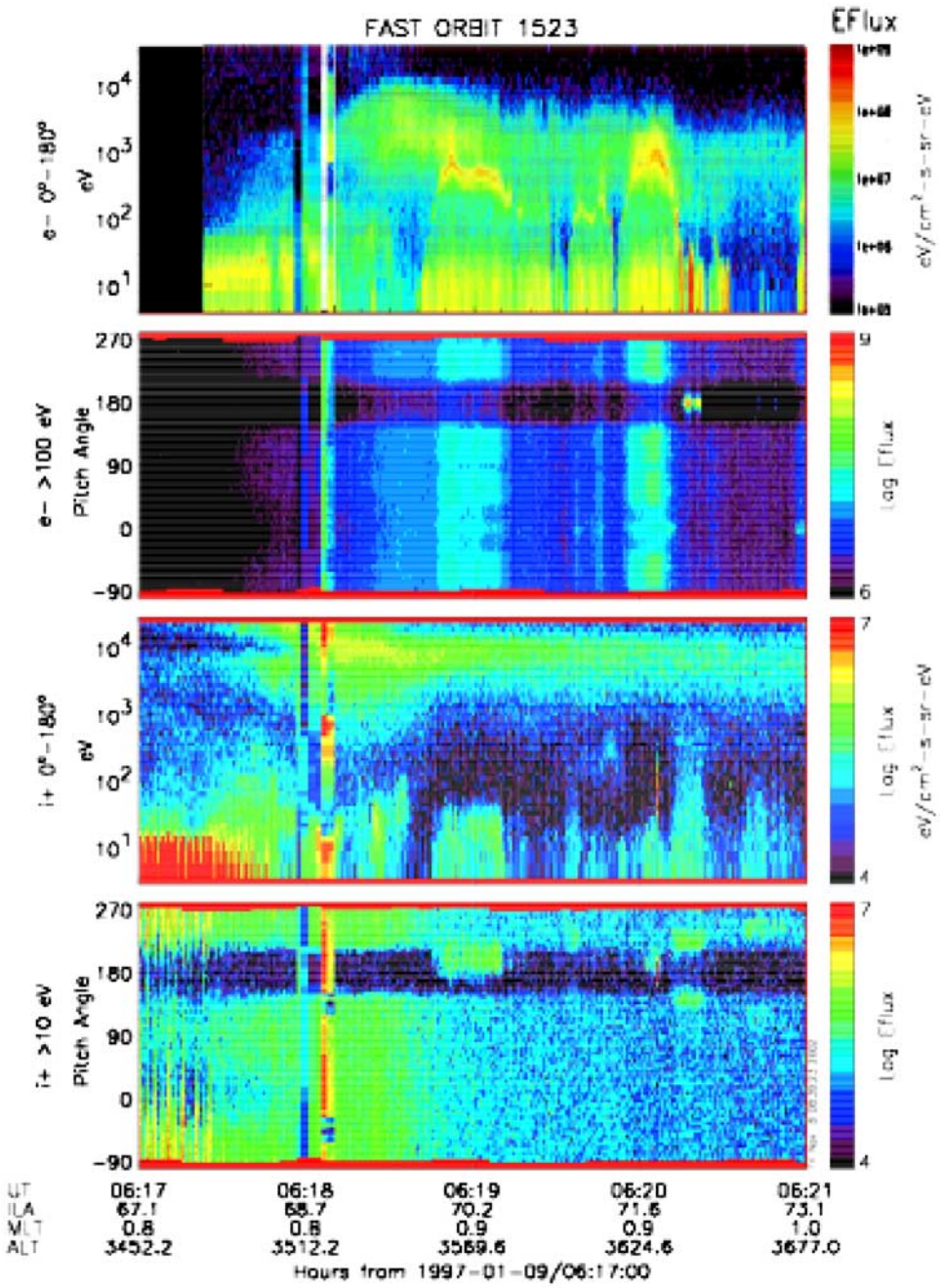

Figure 6. FAST data, obtained just at the start of the growth phase. FAST was located 1 hour to the east of Gillam during this pass. Note the observation of plasma sheet electrons and the weak inverted V precipitation near 0618:50.

energy; the bottom panel shows the ratio of the emissions, used to represent the relative precipitation energy.

[34] A few points should be noted, the first being the striking uniformity in east-west extent of the arc (the field of view of the camera maps to approximately 0.8 hours in local time), as observed at both local times, approximately an hour apart in UT.

[35] Then, consistent with the conclusions drawn using the photometer data, the different traces show that the intensities in both channels have increased by nearly a factor of two in the course of the hour. Accordingly, the third panel shows that the sum of the emissions has likewise increased by the same factor. Finally, the bottom panel shows that the ratio of emissions has changed little, but certainly has not decreased during the hour. Essentially, these data provide a different method of representing the stationarity and gradual intensification of the growth phase arc.

[36] Finally, FAST observations acquired at 0414 UT while located ~2 hours east of Gillam are shown in Figure 10. The stationarity of the arc as shown by the all-sky camera data imply that the FAST observations acquired during this traversal represent a valid measurement of the growth phase arc.

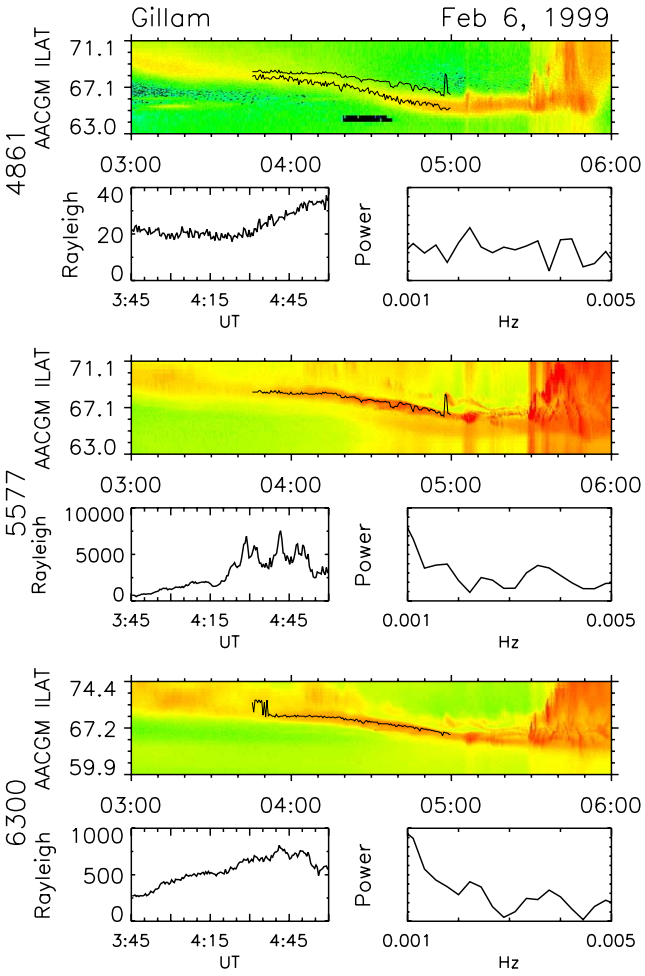

Figure 7. Scanning photometer data for the event on 6 February 1999, plotted in the same format as in Figure 2.

[37] The scanning photometer observations of 4861 Å emissions show variations in latitudinal width, ranging from a fraction of a degree up to ~1°, while FAST observations show the width of proton precipitation to be only ~0.7°, a difference that likely results from the 2-hour longitudinal separation of FAST and Gillam for this event. A similar situation exists with the electron precipitation observations, shown to be only 0.6° wide by FAST, but nearly a degree as observed in 5577 Å emissions. As in the two previous events, the separation in latitude between the 4861 Å and 5577 Å emissions is clear, although in this case the separation increases throughout the growth phase from 0.5 to 1.5° as seen on the ground, but less than 0.5° as observed by FAST.

[38] As expected based on the photometer data, the electron precipitation, marked with an arrow in the figure, occurs just poleward of the proton precipitation, observed from 0414:20 to 0414:40 UT. Unlike the FAST data for the second event, however, the signature of scattered plasma sheet electrons (isotropic distribution with unstructured precipitation) is absent. Instead, a distinct inverted V can be seen in this case. Note that the other difference between these two events is that the growth phase appears to be somewhat more developed in this case, as indicated by the beginning of equatorward motion of the arc precisely at this time. Actually, it may be the case that at the location of FAST that the equatorward motion is more pronounced than shown here. Finally, note that the inverted V structure in electron precipitation with the lack of upflowing ions suggests that the potential drop responsible for the inverted V exists at an altitude above that of FAST (~700 km).

2.4. Event 4: 26 September 1997

[39] The final event to be presented is associated with a very weak, but distinct, substorm. While the event only produced a negative bay of ~80 nT, all of the substorm processes appeared to be operating as usual. Figure 11 shows the scanning photometer data, plotted in the usual format. While the intensity in the 6300 Å channel is seen to increase, the other channels remain virtually constant. Data extracted from the all-sky camera in the same manner as for the previous event show, consistent with the scanning photometer data, that the 6300 Å emissions do intensify (see Figure 12). Note that the all-sky data show that this arc brightens over its entire extent, rather than within a local-

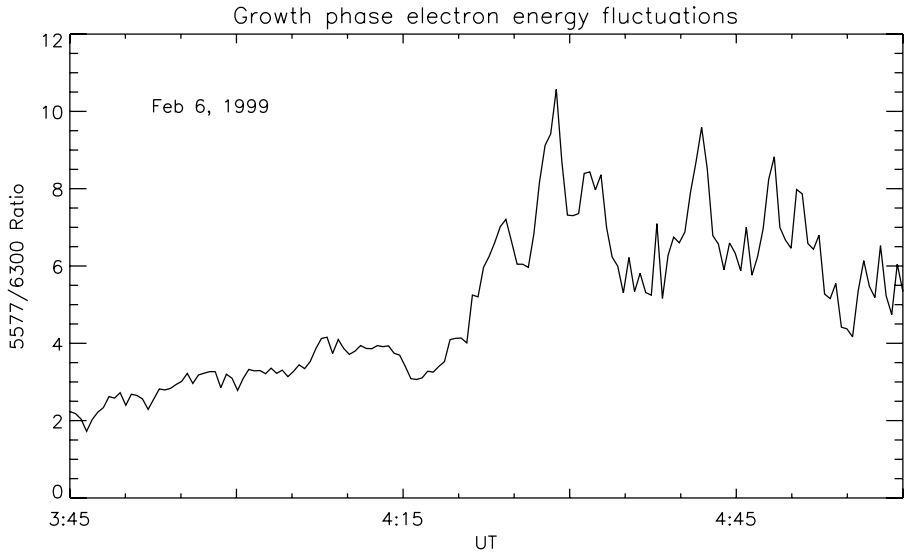

Figure 8. The ratio of I(5577 Å)/I(6300 Å) emissions for 6 February 1999.

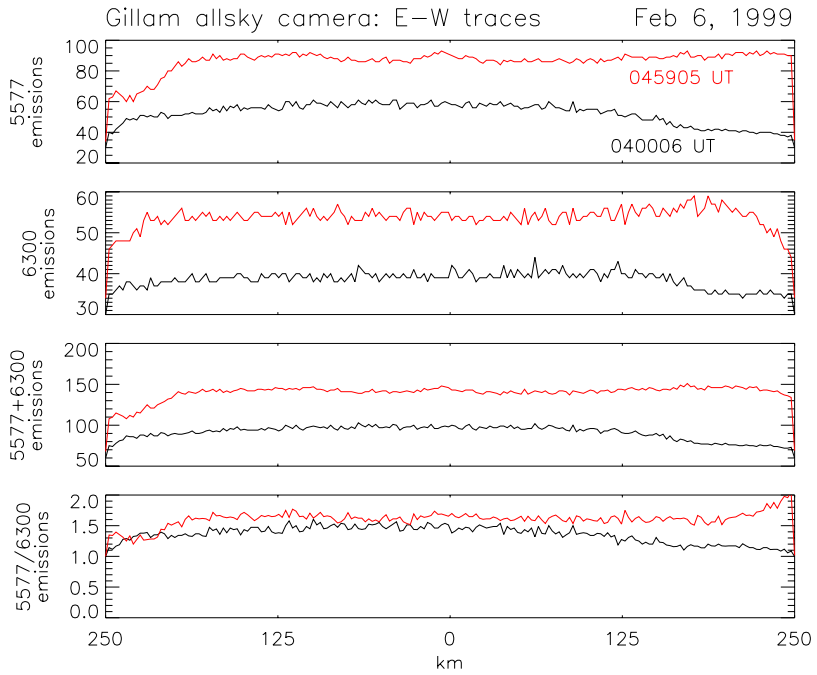

Figure 9. Data extracted from the Gillam all-sky camera observations. Each trace was acquired by extracting the brightest pixel in the north-south direction to yield a measure of arc brightness in the east–west direction. The process was carried out at 5577 and 6300 Å using two separate images, one at 0400:06 UT and then later in the growth phase at 0459:05 UT. Ratios and sums of these emissions are also plotted. The brightness at both wavelengths increases substantially, as does their sum, of course. On the other hand, the ratio increases only moderately, suggesting that an increase in total particle precipitation energy flux resulted from an increase in the number flux, as opposed to the particle energies.

ized region overhead. As in event 3, the magnetometer data show the strongest electrojet signatures along the Churchill line, although it is not possible to definitively determine the precise location of onset, either from the all-sky camera data or otherwise, suggesting the possibility that onset occurred some distance away, as in event 1. Finally, the scanning photometer data show that the 5577 Å and 4861 Å arcs are virtually collocated in this case, unlike the other events presented in this paper.

[40] In spite of the relatively unremarkable activity during this event, HF radio wave data clearly indicate that ionospheric conductivity changes at the very beginning of the growth phase. Figure 13 shows high-frequency wave data recorded by a receiver located at Baker Lake, Nunavit. Baker Lake is nearly along the same magnetic meridian but is well to the north of Gillam. The dark regions shown in the figure represent radio wave power received at Baker Lake that originated from AM radio stations (the majority of them likely being in the United States) after having bounced (perhaps more than once) from the ionosphere and from the ground. The strength of the reflected signal depends strongly on the electron density where the signal penetrates the *D* or *E* region of the ionosphere. In a sense, then, since the source of the signal is composed of a geographically distributed array which will be reflected at different locations, the strength of the signal represents a measure of relative conductivity integrated over a range of latitudes and longitudes south of the receiving station.

[41] In the plot, the vertical arrow in the greyscale points to a region where a decrease in power can be seen in the higher frequencies, visible as a lightening of the greyscale at ~0600 UT. The line plot shows the power summed over the channels from 3.68 MHz to 4.78 MHz and shows the decrease in power somewhat more clearly. Note that this time corresponds very well to the beginning of the equatorward motion of the growth phase arc.

[42] Finally, the onset of the substorm is clearly visible in the HF data as another increase in conductivity (decrease in HF wave power, due to absorption in the *D* layer) at 0648 UT, precisely when the arc is seen to intensify in the scanning photometer data. This is the well-known effect of substorm correlated absorption [see, e.g., *LaBelle et al.*, 1994; *Milan et al.*, 1995, and references therein]. Note that the onset time in the HF data is roughly 5 min later than as determined with the magnetometer data, an effect that could be either temporal or spatial.

[43] Increases in ionospheric conductivity during substorm growth phases have been observed in riometer data (which indicate *D*/*E* region changes in conductivity) by a few authors [*Hones et al.*, 1971; *Hargreaves et al.*, 1975; *Ranta et al.*, 1981]. *Collis et al.* [1986] compared riometer data to EISCAT radar data in order to make direct comparisons of those signals to the electron flux and energy spectrum inferred from EISCAT data. For the single event that they considered, they concluded that the growth phase was characterized by a progressive intensification of precipitating fluxes with energies a few 10's of keV. This result

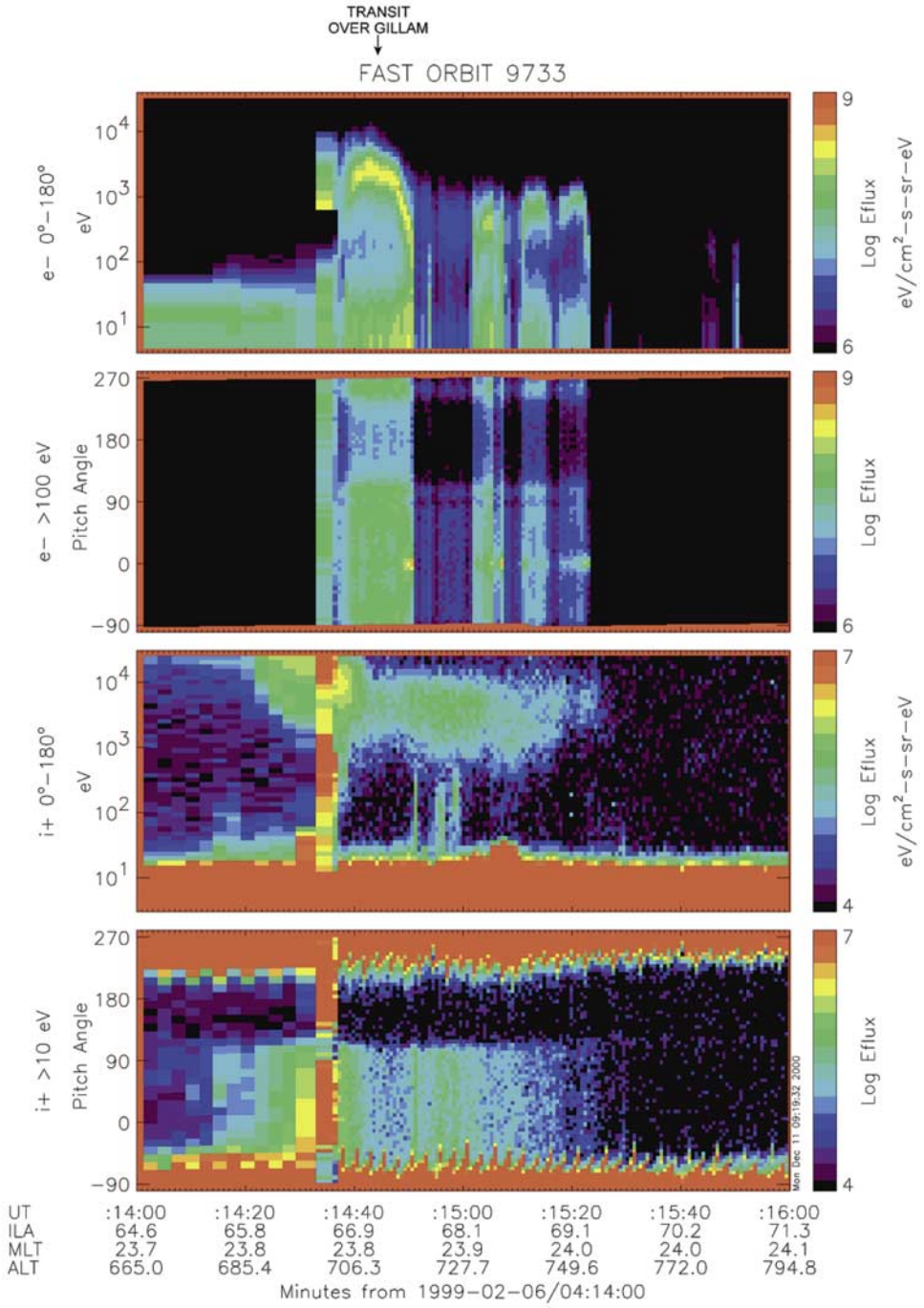

Figure 10. FAST observations acquired at 0414 UT while located ~2 hours east of Gillam.

is consistent with the increased riometer absorption, which is a consequence of effects of the precipitation of particles having energies up to 200 keV [*Collis and Korth*, 1985].

[44] As described above, the CANOPUS scanning photometer data typically show a gradual intensification of luminosity in the 6300 Å and/or 5577 Å channels. While this characteristic is similar to the riometer measurements in the sense that a gradual intensification takes place, it is important to note that the two phenomena are likely not directly related. Specifically, the 6300 Å emissions are associated with electron energies of a few hundred eV and are observed at altitudes of ~230 km, which corresponds to the penetration depth into the upper atmosphere of these particles. The 5577 Å emissions result from somewhat higher energy electrons and are observed at altitudes of ~110 km and higher, also corresponding to the penetration of these electrons into the upper atmosphere.

[45] On the other hand, the HF signature and riometer observations described above map to lower altitudes, typically as low as 80 km. Only more energetic electrons, several 10's of keV and higher, can reach these altitudes. It is this population that is discussed in *Collis et al.* [1986],

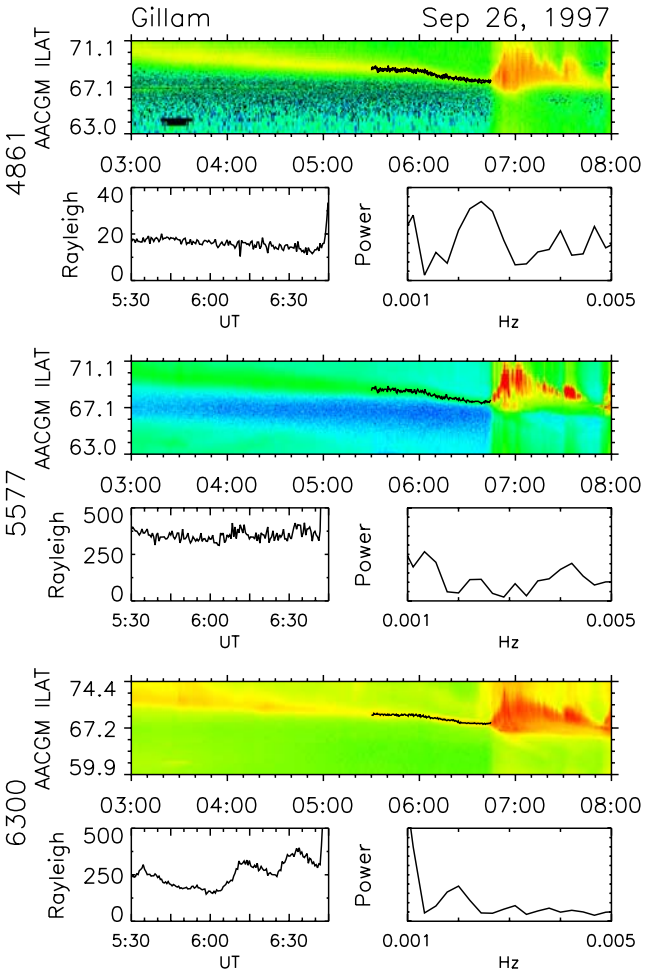

Figure 11. Scanning photometer data for the event on 26 September 1997, plotted in the same format as in Figure 2.

who point out that the accepted mechanism for the effect is that reconfiguration of the magnetic field (i.e., "stretching"), combined with the conservation of the first adiabatic invariant, results in drift shell splitting of the energetic electrons and subsequent spilling into the loss cone [*Baker et al.*, 1981]. Note that this mechanism is unrelated to suggestions that scattering energetic electrons via electron cyclotron harmonic waves may excite diffuse aurora [*Kennel et al.*, 1970; *Scarf et al.*, 1973]. While this latter mechanism has been proposed as appropriate for diffuse aurora, the work of *Baker et al.* [1981] is specifically tied to substorm growth phases and addresses particle distributions observed at geosynchronous orbit during growth phases.

[46] Figure 14 shows FAST data during the first pass of a very fortuitous conjunction. During this traversal, FAST was located just after local magnetic midnight and Gillam was located ~3 hours to the west. The diffuse aurora (i.e., lack of structure) observed at Gillam is consistent with the evidence of scattered plasma sheet electrons and ions observed by FAST. The ion population observed at 68.5°, with pitch angle near 180°, may be an ion conic, though its origin is not clear.

[47] Diffuse aurora is a subject that has been well-studied. *Akasofu* [1964] noted that diffuse aurora was typically present before a substorm, although the concept of a growth phase was not discussed in their work. Global observations of diffuse aurora were presented by *Lui and Anger* [1973], using scanning photometer data from the ISIS-2 satellite and theories for diffuse aurora have been developed, including that of *Chiu and Schultz* [1978] and *Chiu and Cornwall* [1980], discussed below. A main point of this paper is to illustrate that, during the development of a growth phase, auroral luminosity gradually transitions from diffuse aurora to inverted V arcs.

[48] Figure 15 shows the very next pass of the FAST satellite during the same event. During this orbit, it traversed along 23.5 MLT with Gillam at 23.6 MLT, obtaining an excellent measure of the particle fluxes associated with the growth phase. Consistent with other events reported here, the growth phase arc appears to be forming near the poleward edge of the proton precipitation, although the regions of electron and proton precipitation again overlap in latitude. As with the previous event, upflowing ions do not appear with the inverted V electrons, but this time at an altitude of 2800 km, indicating that the acceleration region exists at higher altitudes.

[49] The close Gillam/FAST conjunction provides an ideal opportunity to compare in situ observations of particle precipitation to ground-based observations of luminosity. For both electrons and ions, the second FAST transit (orbit 4335) shows the latitudinal width to be ~0.7°, while the photometer show the widths to be closer to 1°, likely an error that results from a combination of emission lifetimes, an oblique perspective, etc. Also, for this particular event, the emissions appear to be collocated in the photometer data, yet the FAST data show that the peak in electron precipitation is clearly poleward of the proton precipitation, providing an example where examination of the photometer data alone would lead to the wrong conclusion. It is also worth noting that the latitudinal width of the 5577 Å emissions is the order of 2° before the start of the growth phase (i.e., when FAST first passed over Gillam) but gradually decreases to a degree or less when the second pass occurs, with no detectable change in brightness of the emissions.

[50] An important conclusion being drawn in this paper is that the growth phase arc emerges gradually from the scattered electron precipitation. This particular event appears to emphasize this point, with the inverted V forming directly in the region where scattered electrons would normally be found. Note, also, that the energy of the inverted V population is only a few hundred eV, not the more energetic population discussed above.

3. Discussion

[51] One main point resulting from the analysis presented here includes confirmation that growth phase arcs develop in a region near (but within) the poleward edge of proton precipitation. This is not a new result, but the fact that the observations are made using in situ measurements of particle precipitation remove any ambiguities that might result using only observations of luminosity.

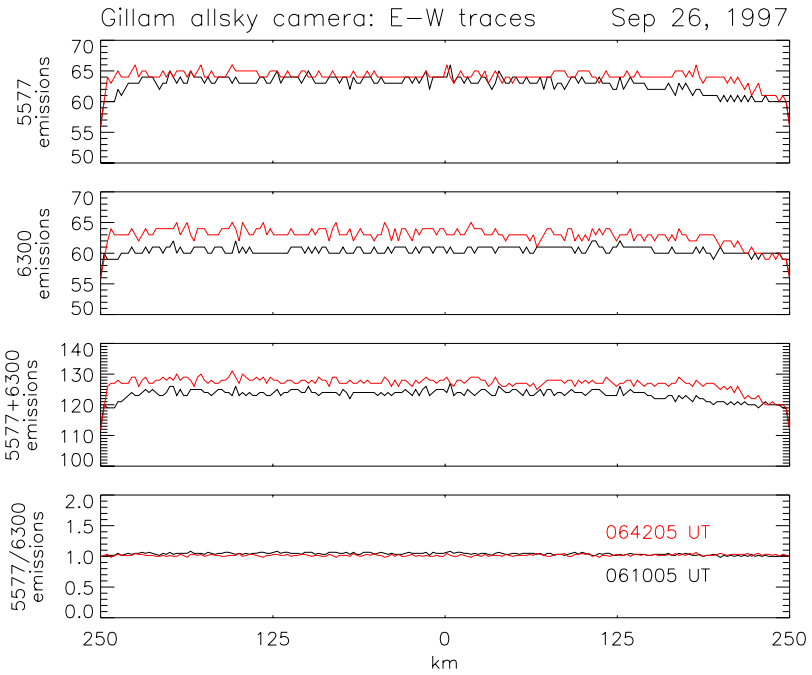

Figure 12. This plot shows traces representing the maximum luminosity in the east-west direction at 0610;05 UT and at 0642:05 UT. These data indicate a slight and gradual increase in precipitating particle energy flux during growth and a uniform arc in local time.

[52] The analysis also leads to new results, including how the stationarity of the arcs suggest that inverted V precipitation evolves from diffuse aurora. Related ionospheric effects are also noted.

3.1. Stationarity of the Arcs

[53] To summarize, of the four isolated growth phase arcs that have been studied, all appear to be stationary for 30 min to 2 hours or more. Luminosity fluctuations (possibly due to field-line resonances) are perhaps present in only one event. Allsky camera data for some of the events showed that the growth phase arcs were uniform in east-west spatial extent over at least 0.75 MLT (limited by the camera field of view), indicating that the electron precipitation was also uniform (in terms of particle energy and precipitation energy flux) over this extent.

3.2. Development of the Inverted V

[54] None of the events examined shows an abrupt change in luminosity that might indicate the abrupt development of an inverted V potential at or near the beginning of the growth phase. The in situ FAST data indicate that the inverted V arcs that do form evolve near the poleward edge of the maximum proton precipitation. Although protons are precipitated over a broad range in latitude, the diffuse 4861 Å emissions that appear (e.g., in scanning photometer data) at the equatorward edge of the oval map to a region in the vicinity of the inner edge of the plasma sheet, where the precipitating proton number flux is greater than what is scattered at higher latitudes. In any case, all data sets in this study show that the growth phase inverted V arcs form within the diffuse electron precipitation; the FAST data also show consistently that the inverted V forms in a region where the electron and proton precipitation overlap.

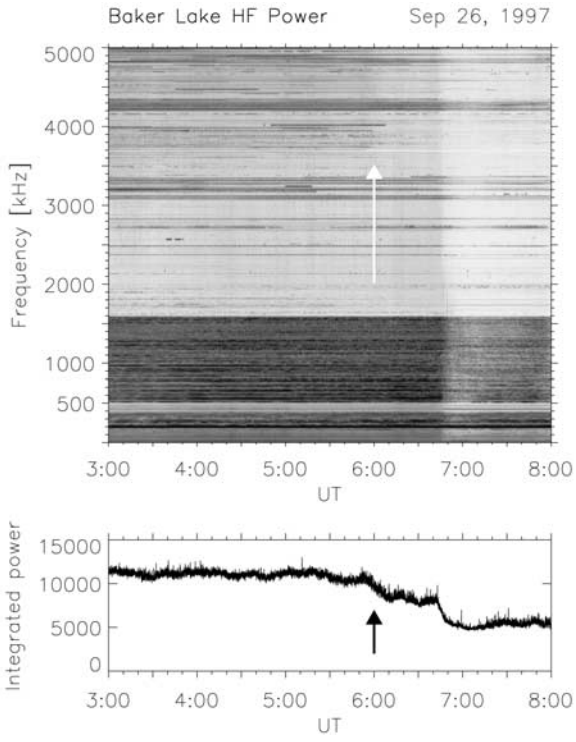

Figure 13. High-frequency radio wave data acquired at Baker Lake, Nunavut, showing an integrated measure of relative conductivity along the Churchill-Gillam meridian. The beginning of the growth phase is seen as a slight fading of the higher frequencies at 0600 UT, which coincides precisely with when the arc began its equatorward drift. Substorm onset is more distinct, occurring at 0648 UT.

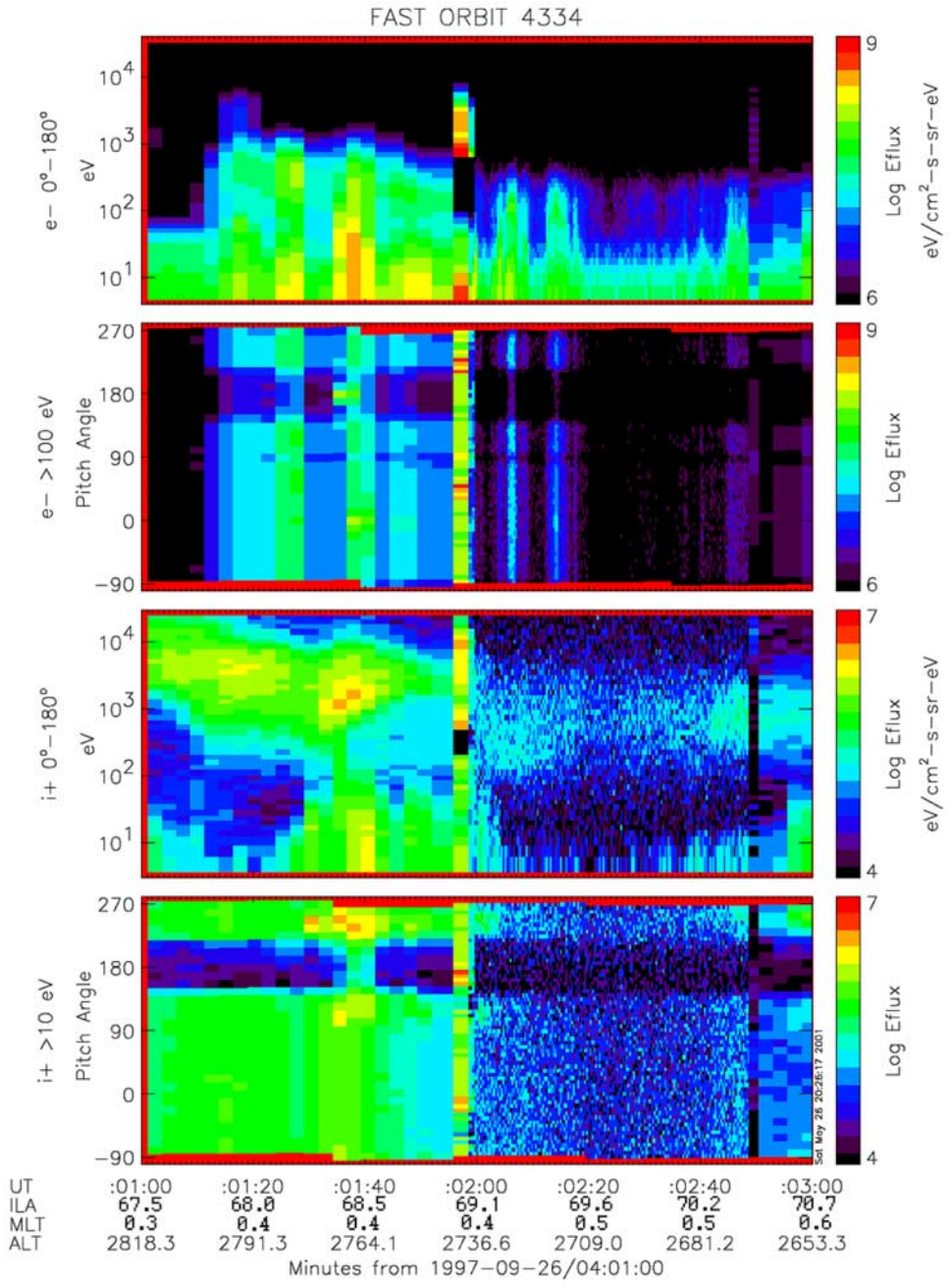

Figure 14. FAST observations approximately well before the beginning of the growth phase. At this time, FAST crossed the auroral zone just after local magnetic midnight, while Gillam was located at approximately 21.5 MLT. The scanning photometer data show only signatures of diffuse aurora; the data in this figure are consistent with Gillam data in that FAST shows evidence of scattered plasma sheet electrons and ions, with no apparent additional acceleration.

[55] To summarize, before the beginning of a growth phase, FAST observations of electron fluxes associated with diffuse aurora (see Figure 14) agree with previous reports [*Deehr et al.*, 1976; *Winningham et al.*, 1978; *Meng et al.*, 1979] in that they typically show a broad energy peak, centered near ~1 keV. Although solid evidence is lacking, a commonly proposed mechanism is that the electrons are scattered from the equatorial region via electron cyclotron harmonic waves. As the growth phase develops, FAST observes the development of a low-energy inverted V that appears to evolve from within the diffuse precipitation. At the same time, as discussed above, drift shell splitting results in the precipitation of particles having energies of 10's of keV. This last point is made for completeness (FAST was not equipped to make such measurements), although we emphasize that the inverted V population is distinct from the energetic particles.

[56] The gradual development and stationarity of the inverted V precipitation combine to place significant constraints on the possible mechanisms responsible for the

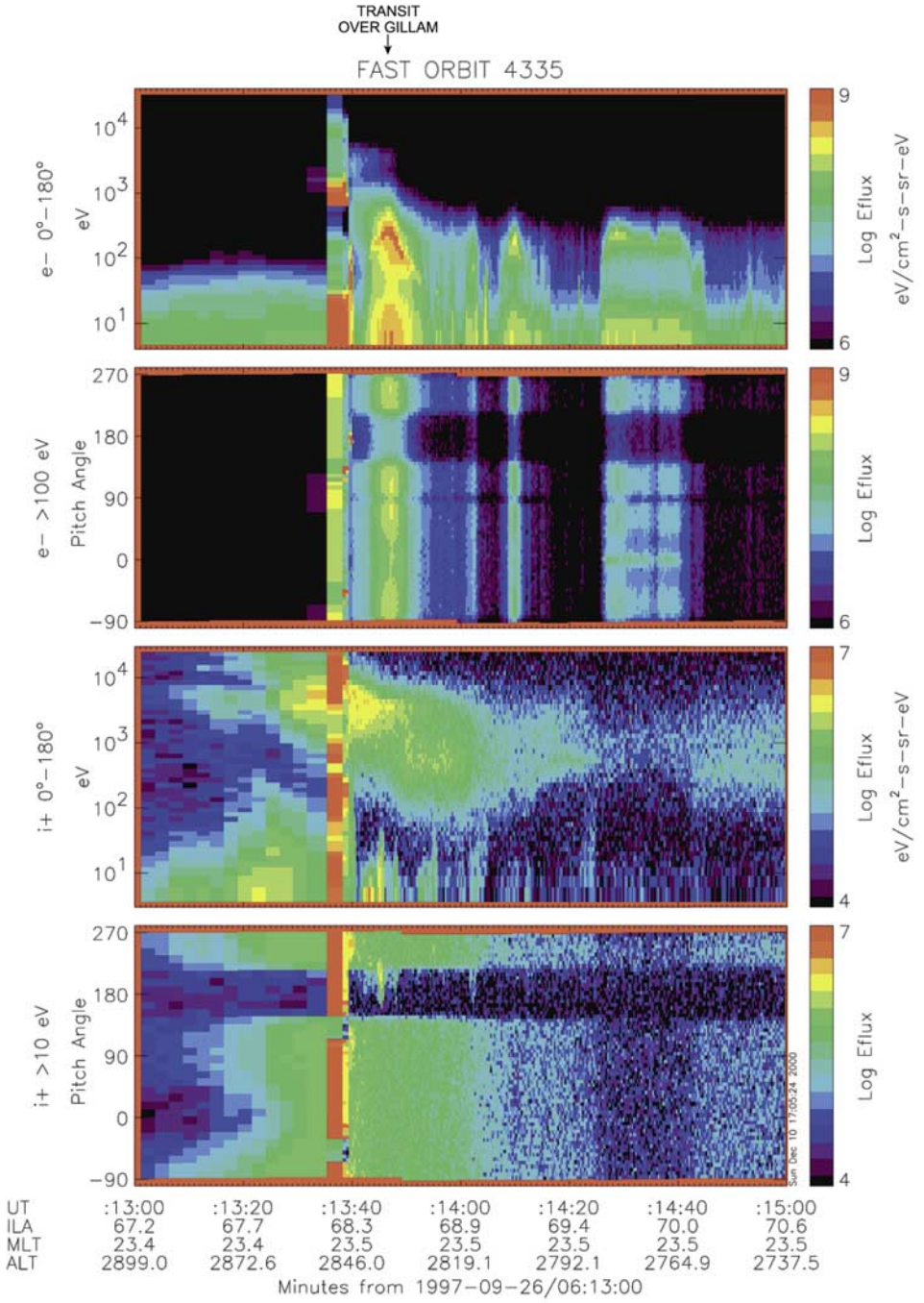

Figure 15. FAST observations directly over Gillam during the growth phase. This fortuitous conjunction shows clearly that the inverted V is forming near the poleward edge of the proton precipitation and that these regions overlap in latitude.

acceleration of these electrons. Specifically, those mechanisms with dynamic characteristics (double layers, Alfvén waves, etc.) do not appear to be relevant. On the other hand, spatial separation of charge along a field line may be a feasible mechanism. *Alfvén and Fälthammar* [1963] pointed out that trapped particles with different energies and pitch angles can establish an electric field. *Persson* [1963] showed that a parallel electric field will be established along a field line unless every element in pitch angle space contains an equal number of ions and electrons. These ideas have since been applied to the magnetosphere and show that the process does indeed support stationary, inverted V arcs [*Chiu and Schultz*, 1978; *Chiu and Cornwall*, 1980]. On the other hand, *Stern* [1981] took a similar approach but allowed for the possibility of discontinuities, violating the quasi-neutrality assumption of *Chiu and Schultz* [1978] and *Chiu and Cornwall* [1980], and also included a gravitational potential barrier, to conclude that double layers may contribute to the formation of the parallel potential drop. Finally, *Janhunen and Olsson* [2000] present model results

from an O-shaped potential structure having a lower region much like a U-shaped structure, associated with waves that feed electrons into the structure. The necessary negative charge cloud (forming the O-shaped potential), in this case, could be supported by mirror effects described above. Yet another possible means of generating stationary arcs is presented by *Knudsen* [1996], who consider effects of plasma drifting through an existing stationary current sheet (which might be provided by the scattered plasma sheet electrons in this case). Effects associated with finite electron inertia, variable plasma density and convective nonlinearities lead to the possibility of parallel electron acceleration in the form of stationary, periodic current sheets. Although this appears to be a viable acceleration mechanism in general, the lack of spatially periodic arcs suggests this mechanism is not responsible for the development of growth phase arcs.

[57] In the cases described here, the inverted V is seen to develop from the overlapping scattered ion and electron plasma sheet populations, where (1) the initial temperatures of these particles are very different (2–20 keV for the ions and 0.4–4 keV for the electrons) and (2) the mechanisms thought to be responsible for scattering the particles from the plasma sheet are very different. Specifically, ions are generally thought to scattered as a result of field-line distortion (i.e., curvature) that develops in a growth phase and electrons are thought to be scattered by electron cyclotron harmonic waves, as described above. The important point is that these particle distributions would have different mirroring characteristics so that, unless the net result of the scattering of the different populations yields identical densities at every point along the field line, the differential mirroring will result in a parallel electric field. The net effect of this process is that a parallel electric field will develop, powered by the processes responsible for scattering the particles from the plasma sheet (e.g., electron cyclotron harmonic (ECH) waves for the electrons). Note that the latitudinal width of the arc would be limited to the region where the mirroring particle populations overlap. Also, note that the energies of the inverted V electrons are below that of the hot plasma sheet electrons (which is typical in all of the cases examined), indicating that the accelerated population is from a cooler population and not directly from the hot plasma sheet population.

3.3. Growth Phase Arcs and Particle Fluxes

[58] Some information about the nature of the growth phase arc can be extracted from the data. *Fridman and Lemaire* [1980] used a kinetic approach to study the relationship between auroral electron fluxes and the associated field-aligned potential drop, beginning with a relationship determined empirically by *Lyons et al.* [1979]. The important conclusion drawn by *Lyons et al.* [1979] is that the net downward electron energy flux varies as V^2, i.e., that the expression $K = \varepsilon/V^2$ describes the relationship between the precipitating particle energy flux and the acceleration potential, with K being a constant. *Fridman and Lemaire* [1980] were able to show that to first order,

$$K = N_e \frac{e^2}{(2\pi m_e)^{1/2}} \frac{\left(E_{0_\parallel}\right)^{1/2}}{E_{0_\perp}} \qquad (1)$$

where $(E_{0_\parallel})^{1/2}/E_{0_\perp}$ represents a measure of the isotropy of the particles, N_e is the electron density in the source region, m_e is the electron mass, and e is the charge.

[59] If the distributions are taken to be isotropic except for the loss cone, which is what the FAST data show, then K simply depends on the source density. The scanning photometer consistently show that the precipitating energy flux increases during growth and is sometimes accompanied by an increase in particle energy. This suggests that the ratio $\varepsilon/V^2 = K$ tends to increase or perhaps remain constant implying that the intensification of the growth phase arc is associated with an increase in the electron density at the source (as opposed to an external intensification of the acceleration mechanism).

3.4. Effect on Ionospheric Conductivity

[60] Four events have been studied in detail, all of which show at least a small increase in luminosity (in the 5777 or 6300 channel or both) during growth, indicating an intensification of the precipitating particle energy fluxes. In two of the events, the ratio of 5577/6300 emissions increases, showing an increase in precipitation energy for these events.

[61] The basic point here is that ionospheric conductivity increases during growth phases. The increase in energy stored in the magnetotail during growth, combined with an increase in conductivity in the region where this energy is ultimately released, implies that conductivity may play a significant role at onset. *Pudovkin* [1991] addressed this question and showed that spontaneous substorms tended to occur more often in cases where the growth phase was well developed, i.e., when the system as a whole became less stable. The results presented in our paper show that this effect likely results from increased conductivity resulting from the gradual intensification of the growth phase arc.

4. Conclusions

[62] Four auroral arcs during substorm growth phases were examined. The analysis combined ground-based data from the CANOPUS chain of stations with FAST overflights (FAST data were available for all but one event). On the basis of the analyses, the following conclusions are obtained, the first two of which are clearly the most significant.

[63] Growth phase arcs in this study last 30 min or more and are typically stationary except for a slow increase in total incident particle energy flux and, possibly, an increase in particle energy. The arcs intensify gradually, with the particle populations evolving from scattered plasma sheet particles to inverted V precipitation.

[64] Growth phase arcs are confirmed using FAST data to form near the poleward edge of proton precipitation. In particular, the arcs appear to form in a region where the scattered electrons and protons overlap. These overlapping populations are likely involved in a differential mirroring process where parallel electric fields may result from a space charge separation.

[65] The increase in particle energy flux and/or particle energies of the precipitating electrons implies that the conductivity of the ionosphere gradually increases during the growth phase. An abrupt increase in conductivity at the beginning of the growth phase was measured, using HF data, during one event.

[66] These arcs are uniform in MLT (within the field of view of the allsky camera, or ~0.75 MLT) in precipitation energy as well as particle energy flux.

[67] The inverted V signatures that develop are consistently of lower energy than the plasma sheet electrons, indicating that these particles are accelerated from a colder population.

[68] In one example, the intensification was observed to occur to the west of the actual onset, raising the question of whether there is a significant difference between an arc that resides somewhat outside the actual onset region and the arc that actually precedes the global onset appearing in the same MLT sector.

[69] **Acknowledgments.** The CANOPUS instrument array constructed, maintained and operated by the Canadian Space Agency, provided data used in this study. Comments from Eric Donovan of the University of Calgary regarding optical data are appreciated. Research at the University of New Hampshire was supported by NASA grant NAG 5-5416. Research at Dartmouth College was supported by NASA grants NNG05GJ70G and NAG 5-7803 and NSF grant ATM-0243595. Research at the University of Washington was supported by NASA grant NAG 5-7732.

[70] Wolfgang Baumjohann thanks Kazuo Shiokawa and another reviewer for their assistance in evaluating this paper.

References

Akasofu, S. I. (1964), The development of the auroral substorm, *Planet. Space Sci.*, *12*, 273.

Akasofu, S. I. (1968), *Polar and Magnetospheric Substorms*, p. 223, D. Reidel, Dordrecht, Holland.

Alfvén, H., and C. G. Fälthammar (1963), *Cosmical Electrodynamics*, pp. 163–167, Clarendon, Oxford.

Baker, D. N., E. W. Hones, P. R. Higbie, R. D. Belian, and P. Stauning (1981), Global properties of the magnetosphere during a substorm growth phase: A case study, *J. Geophys. Res.*, *86*, 8941.

Baker, K. B., and S. Wing (1989), A new magnetic coordinate system for conjugate studies at high latitudes, *J. Geophys. Res.*, *94*, 9139.

Bristow, W. A., G. J. Sofko, H. C. Stenbaek-Nielsen, S. Wei, D. Lummerzheim, and A. Otto (2003), Detailed anaylsis of substorm observations using SuperDARN, UVI, ground-based magnetometers, and all-sky cameras, *J. Geophys. Res.*, *108*(A3), 1124, doi:10.1029/2002JA009242.

Chiu, Y. T., and J. M. Cornwall (1980), Electrostatic model of a quiet auroral arc, magnetotail, *J. Geophys. Res.*, *85*, 543.

Chiu, Y. T., and M. Schultz (1978), Self-Consistent Particle and Parallel Electrostatic Field Distributions in the Magnetospheric-Ionospheric Auroral Region, *J. Geophys. Res.*, *83*, 629.

Collis, P. N., and A. Korth (1985), GEOS-2 observations of energetic electrons in the morning sector during auroral radio absorption events, *J. Atmos. Terr. Phys.*, *47*, 327.

Collis, P. N., S. Kirkwood, and C. M. Hall (1986), D-region signatures of substorm growth phase and onset observed by EISCAT, *J. Atmos. Terr. Phys.*, *48*, 807.

Deehr, C., and D. Lummerzheim (2001), Ground-based optical observations of hydrogen emission in the auroral substorm, *J. Geophys. Res.*, *106*, 33.

Deehr, C. S., J. D. Winningham, F. Yasuhara, and S.-I. Akasofu (1976), Simultaneous observations of discrete and diffuse auroras by the Isis 2 satellite and airborne instruments, *J. Geophys. Res.*, *81*, 5527.

Donovan, E. F., B. J. Jackel, I. Voronkov, T. Sotirelis, F. Creutzberg, and N. A. Nicholson (2003), Ground-based optical determination of the b2i boundary: A basis for an optical MT-index, *J. Geophys. Res.*, *108*(A3), 1115, doi:10.1029/2001JA009198.

Eather, R. H. (1967), Secondary processes in proton auroras, *J. Geophys. Res.*, *72*, 1481.

Erickson, G. M., N. C. Maynard, W. J. Burke, G. R. Wilson, and M. A. Heinemann (2000), Electromagnetics of substorm onsets in the near-geosynchronous plasma sheet, *J. Geophys. Res.*, *105*, 25,265.

Fridman, M., and J. Lemaire (1980), Relationship between auroral electrons fluxes and field aligned electric potential difference, *J. Geophys. Res.*, *85*, 664.

Fukunishi, H. (1975), Dynamic relationship between proton and electron auroral substorms, *J. Geophys. Res.*, *80*, 553.

Hargreaves, J. K., H. J. A. Chivers, and W. I. Axford (1975), The development of the substorm in auroral radio absorption, *Planet. Space Sci.*, *23*, 905.

Hones, E. W., S. Singer, L. J. Lanzerotti, J. D. Pierson, and T. J. Rosenberg (1971), Magnetospheric substorm of August 25–26, 1967, *J. Geophys. Res.*, *76*, 2977.

Janhunen, P., and A. Olsson (2000), New model for auroral acceleration: O–shaped potential structure cooperating with waves, *Ann. Geophys.*, *18*, 596.

Kamide, Y. (2001), Some "missing" elements of constraint in substorm initiation modeling, *J. Atmos. Terr. Phys.*, *63*(7), 635.

Kauristie, K., T. I. Pulkkinen, A. Huuskonen, R. J. Pellinen, H. J. Opgenoorth, D. N. Baker, A. Korth, and M. Syrjasuo (1997), Auroral precipitation fading before and at substorm onset: ionospheric and geostationary signatures, *Ann. Geophys.*, *15*, 967.

Kennel, C. F., F. L. Scarf, R. W. Fredricks, J. H. McGhee, and F. V. Coroniti (1970), VLF electric field observations in the magnetosphere, *J. Geophys. Res.*, *75*, 6136.

Knudsen, D. J. (1996), Spatial modulation of electron energy and density by nonlinear stationary Alfvén waves, *J. Geophys. Res.*, *101*, 10,761.

LaBelle, J., A. T. Weatherwax, M. L. Trimpi, R. Brittain, R. D. Hunsucker, and J. V. Olson (1994), The spectrum of LF/MF/HF radio noise at ground level during geomagnetic substorms, *Geophys. Res. Lett.*, *21*, 2749.

Lui, A., and C. Anger (1973), A uniform belt of diffuse auroral emission seen by the ISIS–2 scanning photometer, *Planet. Space Sci.*, *21*, 799.

Lui, A. T. Y., and J. S. Murphree (1998), A substorm model with onset location tied to an auroral arc, *Geophys. Res. Lett.*, *25*, 1269.

Lyons, L. R., D. S. Evans, and R. Lundin (1979), An observed relation between magnetic field aligned electric fields and downward electron energy fluxes in the vicinity of auroral forms, *J. Geophys. Res.*, *84*, 457.

Lyons, L. R., I. O. Voronkov, E. F. Donovan, and E. Zesta (2002), Relation of substorm breakup arc to other growth phase auroral arcs, *J. Geophys. Res.*, *107*(A11), 1390, doi:10.1029/2002JA009317.

Maynard, N. C., W. J. Burke, E. M. Basinska, G. M. Erickson, W. J. Hughes, H. J. Singer, A. G. Yahnin, D. A. Hardy, and F. S. Mozer (1996), Dynamics of the inner magnetosphere near times of substorm onsets, *J. Geophys. Res.*, *101*, 7705.

McPherron, R. L. (1970), Growth phase of magnetospheric substorms, *J. Geophys. Res.*, *75*, 5592.

Meng, C. I., B. Mauk, and C. E. McIlwain (1979), Electron precipitation of evening diffuse aurora and its conjugate electron fluxes near the magnetic equator, *J. Geophys. Res.*, *84*, 2545.

Milan, S. E., T. B. Jones, M. Lester, E. M. Warrington, and G. D. Reeves (1995), Substorm correlated absorption on a 3200 km trans–auroral HF propagation path, *Ann. Geophys.*, *14*, 182.

Persson, H. (1963), Electric field parallel to the magnetic field in a low–density plasma, *Phys. Fluids*, *9*, 1090.

Pudovkin, M. I. (1991), Physics of magnetospheric substorms: A review, in *Magnetospheric Substorms*, *Geophys. Monogr. Ser.*, vol. 64, edited by J. R. Kan, T. A. Potemra, S. Kokubun, and T. Iijima, p. 17, AGU, Washington, DC.

Pudovkin, M. I., S. I. Isaev, and S. A. Zaitseva (1970), Development of magnetic storms and the state of the magnetosphere according to the data of ground–based observations, *Ann. Geophys.*, *26*, 761.

Ranta, H., A. Ranta, P. N. Collis, and J. K. Hargreaves (1981), Development of the auroral absorption substorm - Studies of pre-onset phase and sharp onset using an extensive riometer network, *Planet. Space Sci.*, *29*, 1287.

Safargaleev, V., W. Lyatsky, and V. Tagirov (1997), Luminosity variations in several parallel auroral arcs before auroral breakup, *Ann. Geophys.*, *15*, 959.

Samson, J. C., L. R. Lyons, P. T. Newell, F. Creutzberg, and B. Xu (1992), Proton aurora and substorm intensifications, *Geophys. Res. Lett.*, *19*, 2167.

Scarf, F. L., R. W. Fredricks, C. F. Kennel, and F. V. Coroniti (1973), Satellite studies of magnetospheric substorms on August 15, 1968, *J. Geophys. Res.*, *78*, 3119.

Steele, D. P., and D. J. McEwen (1990), Electron auroral excitation efficiencies and intensity ratios, *J. Geophys. Res.*, *95*, 10,321.

Stern, D. P. (1981), One-dimensional models of quasi-neutral parallel electric fields, *J. Geophys. Res.*, *86*, 5839.

Vallance Jones, A., F. Creutzberg, R. L. Gattinger, and F. R. Harris (1985), Auroral studies with a chain of meridian scanning photometers 1. Observations of proton and electron aurora in magnetospheric substorms, *J. Geophys. Res.*, *90*, 4489.

Voronkov, I., E. Friedrich, and J. C. Samson (1999), Dynamics of the substorm growth phase as observed using CANOPUS and SuperDARN instruments, *J. Geophys. Res.*, *104*, 28,491.

Winningham, J. D., C. D. Anger, G. G. Shepherd, E. J. Weber, and R. A. Wagner (1978), A case study of the aurora, high-latitude ionosphere, and particle precipitation during near-steady state conditions, *J. Geophys. Res.*, *83*, 5717.

Yago, K., K. Shiokawa, K. Hayashi, and K. Yumoto (2005), Auroral particles associated with a substorm brightening arc, *Geophys. Res. Lett.*, *32*, L06104, doi:10.1029/2004GL021894.

C. W. Carlson, Space Sciences Laboratory, University of California, Berkeley, Berkeley, CA 94720, USA. (cwc@ssl.berkeley.edu)

F. Creutzberg, Keometrics, Ottawa, Ontario, Canada K1J 6C7. (creutzberg@rogers.com)

J. LaBelle, Department of Physics, Dartmouth College, HB 6127, Hanover, NH 03755–6127, USA. (james.labelle@Dartmouth.edu)

M. R. Lessard, Space Science Center, 417 Morse Hall, University of New Hampshire, Durham, NH 03824, USA. (marc.lessard@unh.edu)

W. Lotko, Thayer School of Engineering, Dartmouth College, HB 8000, Hanover, NH 03755–8000, USA. (william.lotko@dartmouth.edu)

W. Peria, Department of Earth and Space Sciences, University of Washington, Box 351650, Seattle, WA 98195–1650, USA. (peria@geophys.washington.edu)

D. D. Wallis, Magnametrics, Ottawa, Ontario, Canada K1J 6C7. (dwallis@eisa.com)